Size Dependence of Gas Sensitivity of ZnO Nanorods

ARTICLE *in* THE JOURNAL OF PHYSICAL CHEMISTRY C · JANUARY 2007

Impact Factor: 4.77 · DOI: 10.1021/jp065963k

Size Dependence of Gas Sensitivity of ZnO Nanorods

L. Liao, H. B. Lu, J. C. Li,* H. He, D. F. Wang, D. J. Fu, and C. Liu

Department of Physics and Key Laboratory of Acoustic and Photonic Materials and Devices of Ministry of Education, Wuhan University, Wuhan 430072, China

W. F. Zhang

Department of Physics, University of Science and Technology of China, Hefei 230026, China

Received: September 12, 2006; In Final Form: November 13, 2006

We report the structure, optical, and gas-sensing properties of ZnO nanorods with different diameters. Vertically well-aligned homogeneous nanorods were grown along the *c*-axis orientation. The shift of Raman scattering E_2 (high) mode and photoluminescence (PL) spectra were used to study the dependences of nanorod diameters on the stress and oxygen vacancy. Gas sensors were prepared and tested for the detection of C_2H_5OH and H_2S (100 ppm) in air. It was found that the thin nanorods have a significantly better sensing performance than the thick nanorods. We provide a possible explanation from the aspect of the sensing mechanism of the surface reaction process.

1. Introduction

In the past decade, one-dimensional (1-D) nanostructures, such as carbon nanotubes,[1,2] ZnO,[3,4] In_2O_3,[5] and SnO_2[6], have attracted much attention because of their potential applications in many fields. Recently, gas sensors based on carbon nanotubes,[7] SnO_2 nanowires,[8,9] and In_2O_3 nanowires[10] were reported. These sensors have excellent response and recover characteristics. However, they are not convenient for mass production.[11]

As an *n*-type semiconductor, ZnO has been extensively used as a gas sensing material due to its high mobility of conduction electrons and good chemical and thermal stability under the operating conditions of sensors.[3,12] It is known that the sensing mechanism of ZnO belongs to the surface controlled type,[13,14] in which the grain sizes, surface states, and oxygen adsorption quantities play important roles in its gas sensitivity. Up to now, most of these studies have focused on ZnO thin films at high temperatures.[15−17] In several recent papers,[18−20] ZnO nanostructures have been reported to demonstrate good sensitivity as sensing materials. But, the key factors of its gas sensing have not been thoroughly studied.

In this paper, well-aligned ZnO nanorod arrays with different diameters were fabricated on Si(100) substrates without using a catalyst. The influences of the structure of ZnO nanorods and defects as well as the related electron donors on their physical properties, surface adsorptions of oxygen, and testing gas, as well as gas sensing characterization, were investigated. The results in this work indicate that the thinner ZnO nanorod arrays could be more sensitive as gas sensors owing to larger adsorption quantities of gas due to more electron donors and a higher surface-to-volume ratio as well as stronger surface effects as compared to thicker nanorods.

2. Experimental Procedures

The ZnO nanorods were prepared by reactive vapor deposition of pure Zn powder in an oxygen-containing ambience as described previously.[21] Si(100) *p*-type substrates were etched using hydrofluoric acid for about 10 min and ultrasonically cleaned by deionized water and ethanol in sequence. The clean silicon substrates were placed on a quartz boat, and the distances between substrates and Zn powder (with a purity of 99.99%) were about 8−10 cm and 4−7 mm for sample A (sample C) and sample B (sample D), respectively. Thus, the ZnO nanowires with different diameters could be obtained. The quartz boat was transferred into the center of the tube furnace. The system was vacuumized by a mechanical pump to a base pressure of about 5 Pa. Argon was then introduced into the system with a flow rate of 70 sccm as the carrier gas, and air (80 sccm) was put into the system as the reactant gas. The system was maintained at 20 Pa. Afterward, the tube was heated to 480 °C (500 °C) at a rate of 25 °C min^{-1} for samples A and B (samples C and D). The reaction lasted for about 60 min. After the furnace cooled down, a white layer was deposited on the substrates.

Figure 1. Schematic diagram of the configuration of the ZnO nanorod array sensor.

The morphologies and crystalline structures of ZnO nanorods were characterized by a Sirion FEG SEM and X-ray diffraction (XRD) using a D8 Advanced diffractometer with a Cu Kα line. Room-temperature Raman scattering was performed in a backscattering geometry by a Renishaw (RM-1000) Raman microspectroscope using an Ar^+ laser (514.5 nm). The PL spectra were measured using a He−Cd laser (325 nm) as the excitation source.

The configuration of ZnO nanorod sensors is shown in Figure 1, which consists of a low-resistance Si substrate as one of the electrodes and a Cu slide as the other electrode pressed on the ZnO nanorods arrays. To improve the contact between ZnO nanorods and Cu electrode, a very thin In film was formed below

* Corresponding author. Tel: +86-27-6875-2567. E-mail: jcli@acc-lab.whu.edu.cn.

10.1021/jp065963k CCC: $37.00
Published on Web 01/18/2007

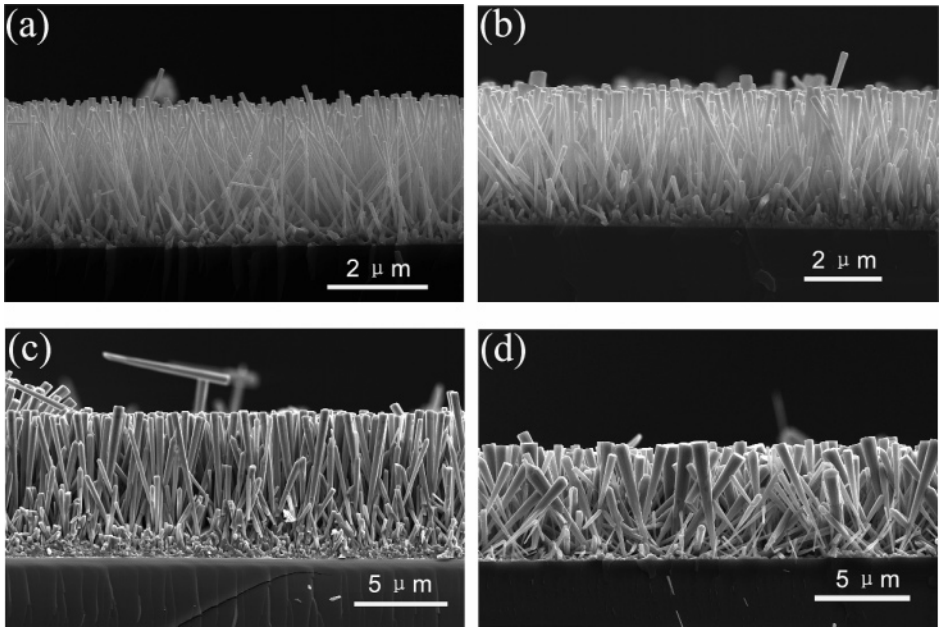

Figure 2. SEM images of ZnO nanorods with diameters of 100 nm (a), 200 nm (b), 400 nm (c), and 800 nm (d).

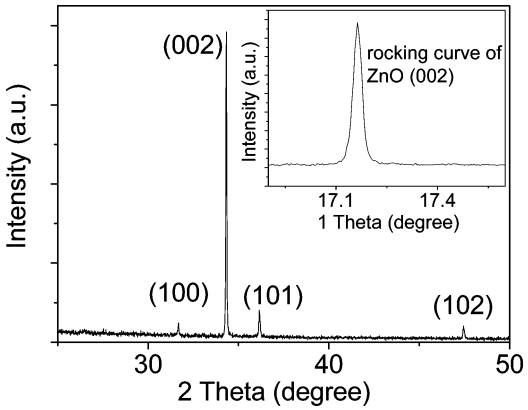

Figure 3. XRD pattern of sample D, the inset showing the X-ray rocking curve of ZnO nanorod arrays [(002) plane].

the Cu. Gas sensing properties of the samples were examined for the gases of C_2H_5OH (100 ppm) and H_2S (100 ppm) in air at 100 °C (for activating chemisorption of the ambient gas components), respectively. The sample resistance was measured by a Kiethley 2400 electrometer as a function of time. The response was defined as the ratio of the electrical resistance in air (R_a) to that in tested gas (R_g) in order that the influence of the reaction area could be ignored.

3. Results and Discussion

As-grown nanorods with different mean diameters, measured by SEM, were sorted out into different groups: about 100 nm (sample A), 200 nm (sample B), 400 nm (sample C), and 800 nm (sample D). The SEM images in Figure 2 show the well-aligned ZnO nanorod arrays with four kinds of different diameters. Figure 3 presents the XRD spectrum of representative sample D. The diffraction peaks can be indexed to a hexagonal wurtzite structure. The inset demonstrates that the full width at half-maximum (fwhm) of the X-ray rocking curve of the (002) peak is as narrow as 0.04°. This provides further statistical evidence that the nanorods grow along the *c*-axial 1-D growth direction.[3]

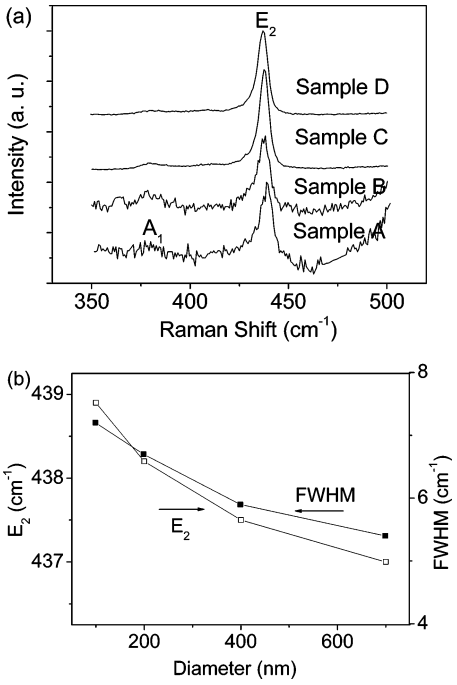

Figure 4. (a) Raman spectra of ZnO nanorod samples and (b) E_2 peak position and fwhm of samples as a function of nanorod diameter.

The micro-Raman peaks of ZnO nanorods at ~383 and ~437 cm^{-1} are clearly observed in Figure 4. The peak at 437 cm^{-1} is attributed to ZnO nonpolar optical phonons high E_2 mode, while the peak at 383 cm^{-1} corresponds to A_1 symmetry with the TO mode. For samples A−D, the position of A_1 (TO) nearly remains unchanged, but that of E_2 (high) shows a shift toward a high frequency (from 437 to ~439 cm^{-1}) with a decreasing diameter of the ZnO nanorod. Such a shift cannot be attributed to the quantum confinement effect of an optical phonon since all these samples' nanorods have a radius larger than the bulk ZnO excitron Bohr radius (~2.34 nm[22]). The E_2 mode (high) is usually used to analyze the stress state in films due to its high sensitivity to stress.[23] The frequency shift of the E_2 mode (high) may be attributed to the stress variation. Since the E_2 mode

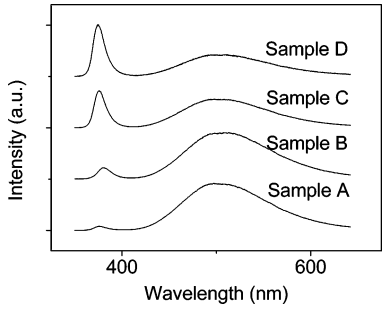

Figure 5. Photoluminescence spectra of samples.

(high) of sample D is much closer to that (437 cm^{-1})[24] of bulk ZnO, the stress within the sample D with the largest diameter of nanorods can be neglected. Decremps[25] reported that under pressure, the E_2 (high) frequency of the wurzite ZnO crystal blue-shifted from that of free pressure and increased with the increase of biaxial compressive stress within the *c*-axis oriented ZnO epilayers. In our cases, the E_2 (high) frequencies of samples A−C are all higher than that of sample D, which demonstrates that samples A−C are under compressive stress and that sample A (100 nm) possessing the largest frequency (see Figure 4b) of the E_2 mode(high) undergoes the largest compressive stress than samples B (200 nm), C (400 nm), and D (800 nm). The more compressive stress could bring more defects (such as oxygen vacancy (V_o), etc.) in ZnO nanorods, and this argument could also be supported by the PL results (sample A has the largest intensity of green emission broadbands related to V_o) shown in Figure 5 and by the observation that the fwhm of E_2 (high) increases with the decrease of the nanorod diameter, as shown in Figure 4b, because the increase of fwhm of E_2 (high) means the degeneration of crystalline quality[26] (i.e., the increase of defects).

The PL spectra of the samples are shown in Figure 5. All the spectra have a UV emission peak centered at 380 nm corresponding to the near band edge (NBE) emission and a green emission broadband centered at about 500 nm related to the intrinsic defects in the ZnO samples. It is obvious that the intensity of the UV peak decreases while the intensity of the visible broadband increases as the diameters of ZnO nanorods decrease. This means that the concentration of the intrinsic defects in the samples increases when the diameters of the nanorods decrease. Generally, the peak at 500 nm originates from single ionized oxygen vacancies (V_o).[27] The results indicate that the density of V_o increases when the diameter of ZnO nanorods decreases.

Figure 6 shows the typical response curves of the ZnO sensors to C_2H_5OH and H_2S (100 ppm) in air. It can be seen that the sample A sensors have an obviously better sensing performance than the sample D devices, such as a higher C_2H_5OH sensitivity and shorter response time. This enhanced gas sensitivity of the thin ZnO nanorod sensors has also been found in their responses to H_2S gases (shown in Figure 6b). Under the present operating conditions, for all the ZnO nanorod sensors, it has been noticed that the gas sensitivity increases with increasing concentration of gas in air. For observing clearly, only one cycle is laid out. In fact, the 20 cycles were repeated, and the results are the same in Figure 6.

The mechanism of enhanced sensing of thin ZnO nanorod sensors can be explained by the modulation model of the depletion layer[13] as follows shown in Figure 7. The potential barriers at the grain boundaries reduce the carrier mobility. The oxygen vacancy (V_o) in ZnO nanorods acts as an electron donor

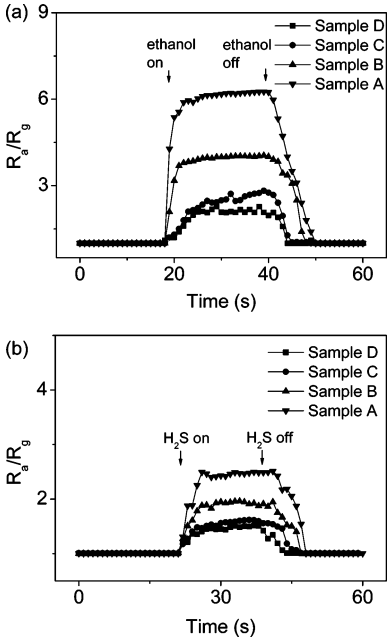

Figure 6. Typical response curves of the four kinds of ZnO nanorod sensors: (a) C_2H_5OH and (b) H_2S.

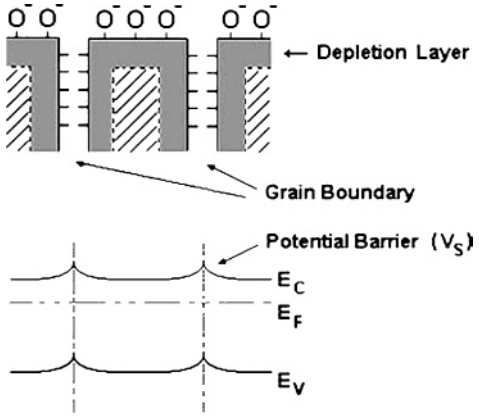

Figure 7. Formation of depletion layers in the surface and grain-boundary regions of ZnO due to oxygen chemisorption.

in ZnO to provide electrons to the conduction band of ZnO and makes ZnO nanorods an *n*-type semiconductor.[28] The exposed surface of nanorod adsorbs the oxygen molecules from the ambient gas components, which capture electrons from the conduction band and form O^-; see eq 1.

$$O_2(g) + 2e^- \rightarrow 2O^-(ads) \quad (1)$$

After sufficient adsorption of oxygen, depletion layers were formed on the surface regions of nanorods, which caused the carrier concentration to decrease and consequently increased the resistance of the nanorod sensor. Intuitively, a larger surface area provides more positions to adsorb oxygen molecules. Furthermore, a larger quantity of V_o induces higher adsorptions of oxygen without lowering the expansion level of depletion layer for as-grown (undoped) ZnO nanorod samples, which results in a further increase of the resistance of nanorod sensors. In addition, the surface effect of nanomaterials, namely, a high surface-to-volume ratio results in the high quantity of surface atoms of thin nanorods, which can lead to the insufficiency of surface atomic coordination and high

surface energy.[29] Therefore, the surfaces are highly active, which promotes further adsorption of oxygen in the ambient atmosphere.

When the sensors are exposed to reducing gases, for instance, ethanol or H_2S, the gas will react with the adsorbed O^-, as in eqs 2 or 3, and release the trapped electrons back to the conduction band. This leads to an increasing carrier concentration of ZnO and decreasing resistances of sensors.[30,31]

$$CH_3CH_2OH(ads) + 6O^-(ads) \rightarrow 2CO_2(g) + 3H_2O(l) + 6e^- \quad (2)$$

$$H_2S(g) + 2O^-(ads) \rightarrow H_2(g) + SO_2(g) + 2e^- \quad (3)$$

Thus, sample A sensors have a significantly better sensing performance than samples B−D sensors due to larger quantity of V_o and higher surface-to-volume ratio, namely, a larger effective surface areas of thinner nanorod arrays.

4. Conclusion

In conclusion, the vertical arrays of well-aligned *c*-axis orientation ZnO nanorods with different diameters have been synthesized by oxygen assisted thermal evaporation of metallic zinc on Si(100) substrates over a large area. Raman scattering reveals that the compressive stress within ZnO nanorods increases with the decreasing diameter of nanorods and consequently increases the defects in the surface layers of the thinner nanorods. The insufficiency of atomic coordination due to the large surface-to-volume ratio is also one of the important factors (growth process, stress, etc.) inducing the increase of V_o in thinner nanorods. The high surface adsorption of oxygen is the key for obtaining an excellent gas sensing performance of the sensor. It was found that the thinner ZnO nanorod sensors have significantly better sensing performance due to a larger quantity of electron donors related to V_o and larger effective surface areas, resulting in a larger quantity of adsorbed oxygen than the thicker nanorod sensors. Therefore, the thin well-aligned ZnO nanorods would be of great potential for many practical applications including gas sensors.

Acknowledgment. This work was supported by the National Natural Science Foundation of China (Grant Nos. 10575078 and 10475063).

References and Notes

(1) Iijima, S. *Nature* **1991**, *354*, 56.
(2) Baughman, R. H.; Zakhidov, A. A.; De Heer, W. A. *Science* **2002**, *297*, 788.
(3) Huang, M.; Mao, S.; Feick, H.; Yan, H.; Wu, Y.; Kind, H.; Weber, E.; Russo, R.; Yang, P. D. *Science* **2001**, *292*, 1897.
(4) Wang, Z. L.; Song, J. H. *Science* **2006**, *14*, 242.
(5) Yu, D. P.; Yu, S. H.; Zhang, S.; Zuo, J.; Wang, D.; Qian, Y. *Adv. Mater.* **2003**, *13*, 497.
(6) Zhang, D. F.; Sun, L. D.; Yin, J. L.; Yan, C. H. *Adv. Mater.* **2003**, *15*, 1022.
(7) Kong, J.; Franklin, N. R.; Zhou, C. W.; Chapline, M. G.; Peng, S.; Cho, K. J.; Dai, H. J. *Science* **2000**, *287*, 622.
(8) Kolmakov, A.; Zhang, Y. X.; Cheng, G. S.; Moskovits, M. *Adv. Mater.* **2003**, *15*, 997.
(9) Wang, Y. L.; Jiang, X. C.; Xia, Y. N. *J. Am. Chem. Soc.* **2003**, *125*, 16176.
(10) Li, C.; Zhang, D. H.; Liu, X. L.; Han, S.; Tang, T.; Han, J.; Zhou, C. W. *Appl. Phys. Lett.* **2003**, *82*, 1613.
(11) Wang, C. H.; Chu, X. F.; Wu, M. M. *Sens. Actuators, B* **2006**, *113*, 320.
(12) Wan, Q.; Li, Q. H.; Chen, Y. J.; Wang, T. H.; He, X. L.; Li, J. P.; Lin, C. L. *Appl. Phys. Lett.* **2004**, *84*, 3654.
(13) Gergintschew, Z.; Förster, H.; Kositza, J.; Schipanski, D. *Sens. Actuators, B* **1995**, *26*−*27*, 170.
(14) Egashira, M.; Shimizu, Y.; Takao, Y.; Sako, S. *Sens. Actuators, B* **1996**, *35*−*36*, 62.
(15) Suchea, M.; Christoulakis, S.; Moschovis, K.; Katsarakis, N.; Kiriakidis, G. *Thin Solid Films* **2006**, *515*, 551.
(16) Christoulakis, S.; Suchea, M.; Koudoumas, E.; Katharakis, M.; Katsarakis, N.; Kiriakidis, G. *Appl. Surf. Sci.* **2006**, *252*, 5351.
(17) Wagh, M. S.; Jain, G. H.; Patil, D. R.; Patil, S. A.; Patil, L. A. *Sens. Actuators, B* **2006**, *115*, 128.
(18) Xu, J.; Pan, Q.; Shun, Y.; Tian, Z. *Sens. Actuators, B* **2000**, *66*, 277.
(19) Law, M.; Kind, H.; Messer, B.; Kim, F.; Yang, P. *Angew. Chem., Int. Ed.* **2002**, *41*, 2405.
(20) Wang, X. H.; Zhang, J.; Zhu, Z. Q. *Appl. Surf. Sci.* **2006**, *252*, 2404.
(21) Liu, D. H.; Liao, L.; Li, J. C.; Guo, H. X.; Fu, Q. *Mater. Sci. Eng. B* **2005**, *121*, 77.
(22) Senger, R. T.; Bajaj, K. K. *Phys. Rev. B* **2003**, *68*, 45313.
(23) Tripathy, S.; Chua, S. J.; Chen, P.; Miao, Z. L. *J. Appl. Phys.* **2002**, *92*, 3503.
(24) Calleja, J. M.; Cardona, M. *Phys. Rev. B* **1977**, *16*, 3753.
(25) Decremps, F.; Porres, J. P.; Saitta, A. M.; Chervin, J. C.; Polian, A. *Phys. Rev. B* **2002**, *65*, 92101.
(26) Santhakumar, K.; Nair, K. G. N.; Kesavamoorthy, R.; Ravichandran, V. *Nucl. Instrum. Methods Phys. Res., Sect. B* **2003**, *212*, 381.
(27) Hu, J. W.; Bando, Y. *Appl. Phys. Lett.* **2003**, *82*, 1401.
(28) Lin, C. C.; Chen, S. Y.; Cheng, S. Y.; Lee, H. Y. *Appl. Phys. Lett.* **2004**, *84*, 5040.
(29) Halperin, W. P. *Rev. Modern Phys.* **1986**, *58*, 533.
(30) Windischmann, H.; Mark, P. *J. Electrochem. Soc.* **1979**, *126*, 627.
(31) Kar, S.; Pal, B. N.; Chaudhuri, S.; Chakravorty, D. *J. Phys. Chem. B* **2006**, *110*, 4605.